Examining PSFs

AS

August 29, 2013

Abstract

Study on behavior of PSF for different data types. Most stress is on usage of PSF as a comparison qualification for comparing different data collection modes.

1 Methods

- Use system matrix for 4 different event type (Si-Si, Si-BGO) X (1.4 mm, 1 mm) pads.
- Generate N=1M background events; add a point source with N_S=2 k events. Point source can appear at different positions in the FOV. Generate data without the source for the same settings (data type, etc.).
- Reconstruct both datasets with MLEM; use the same system matrix as above. Vary number of iterations.
- Subtract background only image from the point source embedded image.
- Study the resulting image.

2 Detectability as a function of distance

Generate point sources with the same amount of events at different distances from the center. The detectability index is defined as a dot product of the resulting reconstructed image with a 2D gaussian with a width of 1 mm sigma centered at the simulated source location. In fact, convolution with the gaussian was performed and content of the histogram at the insertion point was taken as the result of the hypotetical dot multiplication.

3 PSF size as a function of iteration number

As expected, the size of the reconstructed psf is a function of the iteration number. The area was determined from a set of slices through the reconstructed subtraction image of the spot performed at N=8 equally spaced sampling angles. At each slice the resulting profile was fit with a Gaussian function and the diameter was estimated as $2.35\times\sigma$ where σ is the fit width of the Gaussian function. The resulting N diameters were squared, divided by four, multiplied

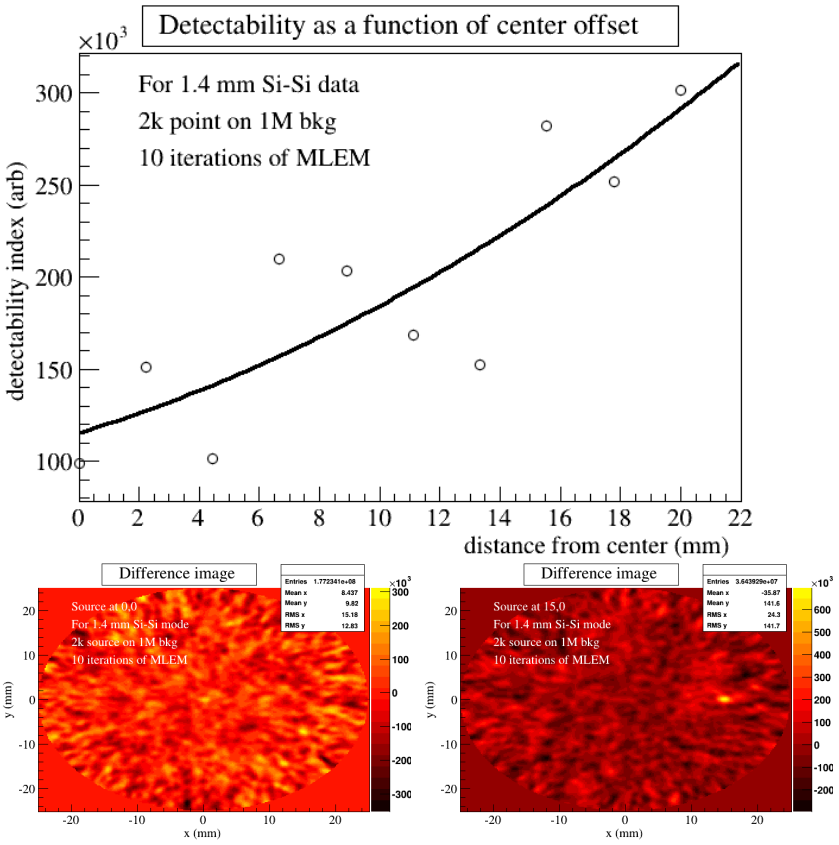

Figure 1: TOP:Detectability index as a function of the distance of the source from the center of the FOV. BOTTOM: Difference images (background subtracted from the background embedded point source) for sources modelled at different locations; FOV origin (left) and 15 mm away from the center (right).

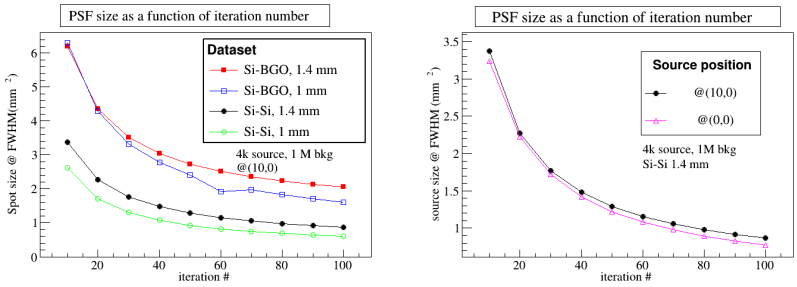

Figure 2: Size of the PSF as a function of the MLEM iteration number. Simulation of the sources superimposed on homogenuous background. Comparison among data types (left) and among different positions in the FOV (right).

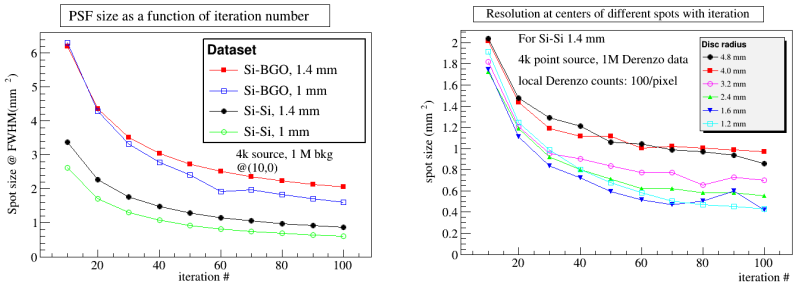

Figure 3: Size of the PSF as a function of the MLEM iteration number. Sources embedded in Derenzo phantom at the centers of the rods with listed diameters. Comparison among data types (left) and among different rods in the phantom (right).

by the angular spacing, and summed to yield an estimate of the reconstructed spot size. A slight variation in spot size in the right part of the Figure indicates that different part of the FOV will have different resolution properties.

Similar pictures are obtained for overlaying a point source on simulated Derenzo data. Here, a striking difference can be observed as point source is moved onto different rods of the phantom. The activity surrounding the investigated pixel leaks onto the PSF of the pixel, making it wider for large rod diameters, and smaller for smaller rods. The effect is nearly saturated below a rod size of 2.4 mm, tailing off to a spot size of 0.4 mm^2, or, assuming a circular shape, a diameter of 0.35 mm at FWHM, still exceeding the bin size of 0.2 mm.

4 Variance vs. PSF size as a function of iteration

To extract relation between variance and PSF the following procedure was employed:

- Generate a base image from Derenzo phantom with N=1M events of which q×N with q=0.1 are background events (why?)

- Select rods of a certain diameter and identify the one closest to the center of the phantom. In this way six locations are obtained, one for each rod diameter
- In each of the six locations from the previous item, generate an additional data set by adding a true, single pixel point source with 4k events to the base image, (local signal to noise is 4000/100). This makes a set of seven sinograms, including the base sinogram.
- Repeat the outlined procedure nSample=10 times. At the outset, nSample*nRods=70 sinograms are generated for each PET layout.
- Iterate over the set of sinograms, processing each independently. Every n=10 iterations examine the set.
- **Spatial resolution**. The set examination begins by, within each sample and for each rod diameter, subtracting the image reconstructed from the base sinogram from the image reconstructed from sinogram with overlaid point source. Each subtraction yields an approximation to the PSF at the given iteration. Since nSample such realizations were constructed, nSample approximations of PSF are available at each iteration. To extract a PSF measure, all realizations are averaged together for each rod diameter to yield nRods averages of PSF. These images are then subject to calculation of the PSF FHWM area as described in previous section.
- **Variance**. The next setp in set examinations is determination of the variance. For this, the nSample images reconstructed from base sinograms are subject to calculation of pixel wise sum of pixel contents and squares of pixel content. The two sums allow to construct pixel wise average and variance of the reconstructed image. A local approximation to variance is obtained by averaging the variance in the neighborhood of the pixel where source was generated and dividing it by average content of the pixels within the hot rods of the phantom. The neighborhood was taken as pixels not further than 1 mm from the pixel with the point source. That amounted to 78 pixels per neighborhood. The variance estimation is somewhat correlated to the choice of neighborhood; its effect is still to be investigated.
- The pair of values - spatial resolution and variance - was stored and iteration continued.

The results show comparison of different datasets. Up to 200 iterations were performed. More might be needed.

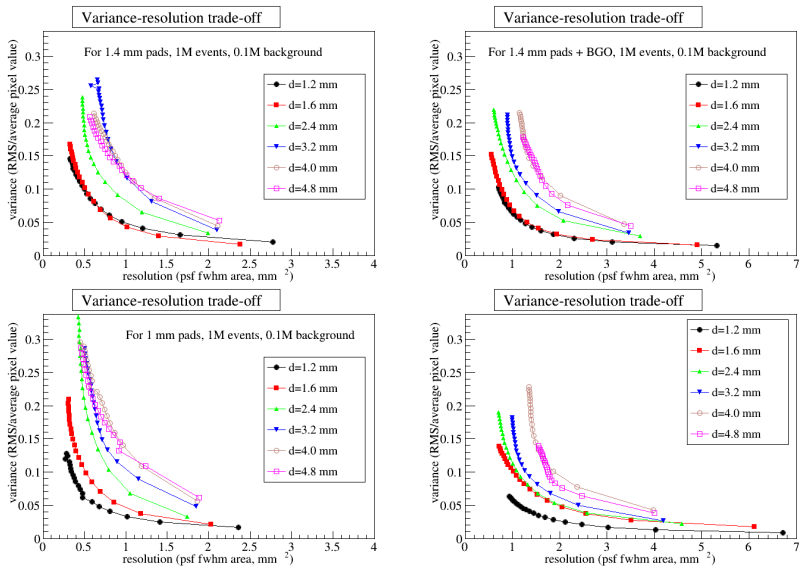

Figure 4: Trade-off for different setups and different regions of the Derenzo phantom. Setups:
TOP LEFT: Si-Si with 1.4 mm pads.
TOP RIGHT: Si-BGO, Si with 1.4 mm pads.
BOTTOM LEFT: Si-Si with 1 mm pads.
BOTTOM RIGHT: Si-BGO, Si with 1 mm pads.
Each graph within the subplot corresponds to the diameter of the rod on whose center a point source was simulated and a sample of variance was extracted. For up to 200 iterations.

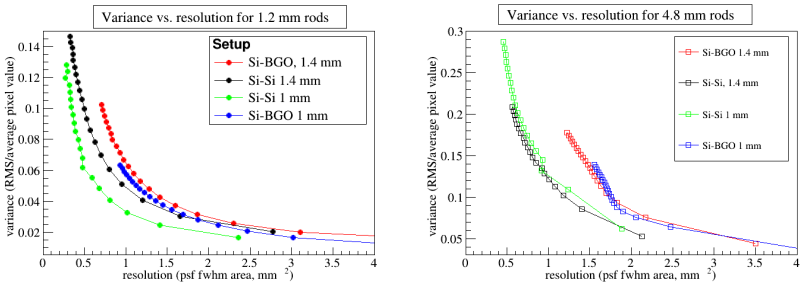

Figure 5: Comparison of performance for different data sets and different locations in the phantom - 1.2 mm rods on left, 4.8 rods on right. According to expectations, the 1 mm detectors in coincidence outperform other modes of data collection when variation of small sources is determined. However, the performance of 1 and 1.4 mm detectors are nearly identical when a small source is overlaid on a large source. No explanations for this pattern yet. Maybe it has to do with FOV area or density of the LOR. Hard to say. Nevertheless, Si-Si is in both cases much better than Si-BGO.

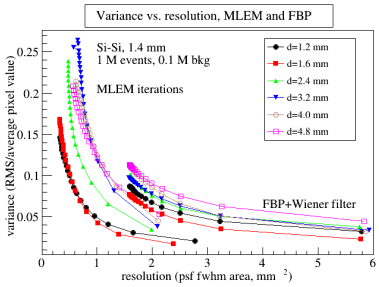

Figure 6: Comparison of performance for different reconstruction methods, FBP and MLEM. The tunning parameter in FBP is the filter shape, in particular cut-off frequency for the Wiener filter, while iterations serve as MLEM tunning parameter. Notice the improved performance of the MLEM routine.

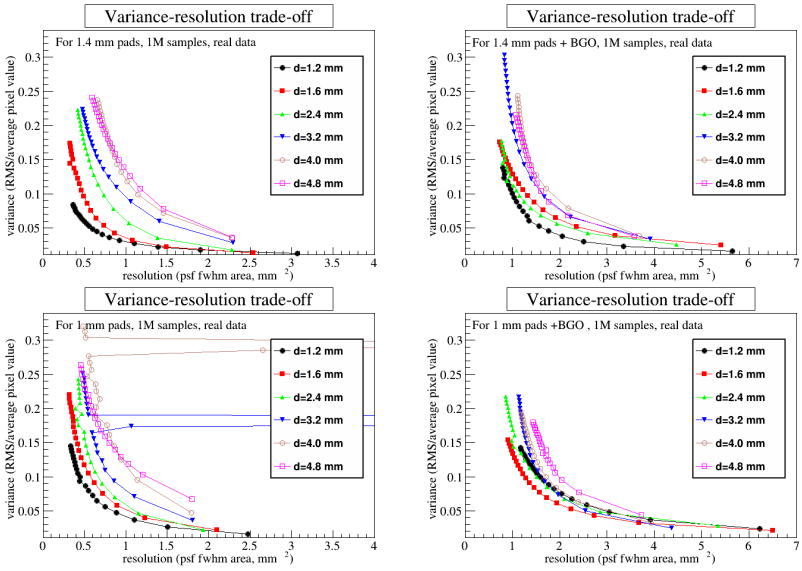

Figure 7: Trade-off for different setups and different regions of the Derenzo phantom. Measured data. Setups:
TOP LEFT: Si-Si with 1.4 mm pads.
TOP RIGHT: Si-BGO, Si with 1.4 mm pads.
BOTTOM LEFT: Si-Si with 1 mm pads.
BOTTOM RIGHT: Si-BGO, Si with 1 mm pads.
Each graph within the subplot corresponds to the diameter of the rod on whose center a point source was simulated and a sample of variance was extracted. For up to 200 iterations.

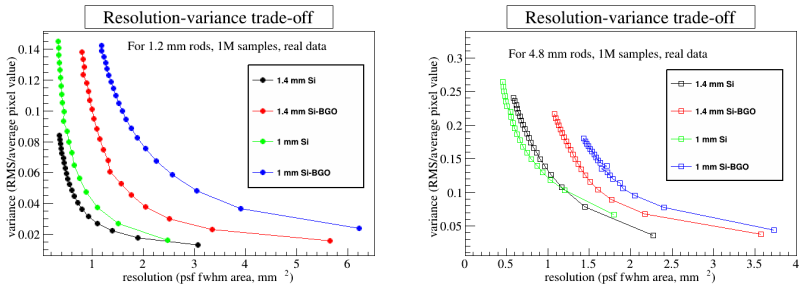

Figure 8: Comparison of performance for different data sets and different locations in the phantom - 1.2 mm rods on left, 4.8 rods on right. For **measured data**.

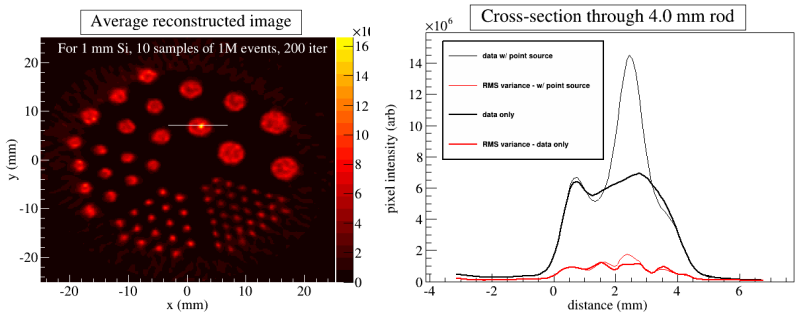

Figure 9: LEFT: Average of a set of reconstructed images with embedded point source on 4.0 mm diameter rod. Position guessed for phantom mechanical layout (slightly wrong, based on reconstruction). Real data for 1 mm Si sensors in coincidence, after 200 iterations of MLEM. RIGHT: Cross-sections through average image on the left along the white line indicated on the left image. Also shown are cross-sections through the pixel-wise RMS variance of the set, and also the same for the unperturbed data w/o the embedded point source.

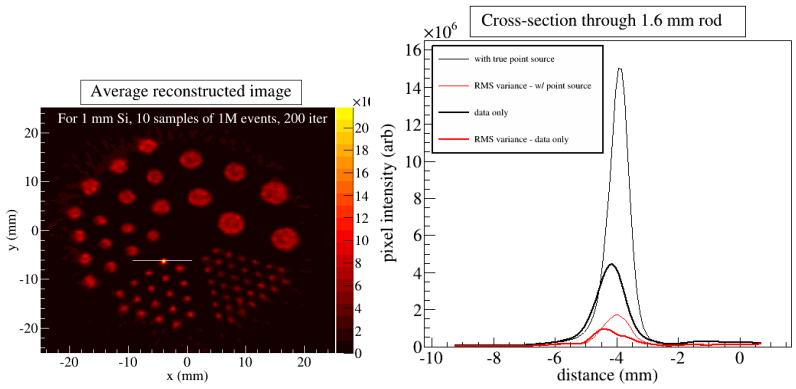

Figure 10: The same as Figure 9, only for 1.6 mm diameter rod.

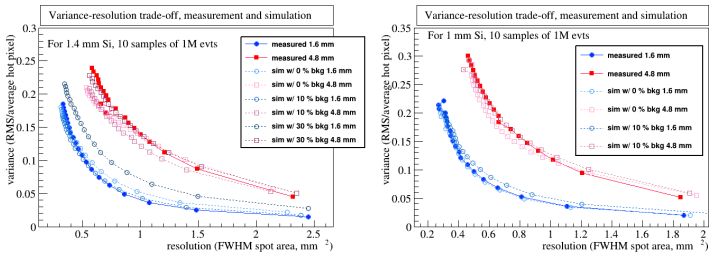

Figure 11: Comparison of simulation and real data. For 1.4 mm (LEFT) and 1 mm Si(RIGHT), 10 samples of 1M events, two rod diameters and different amount of added background (no background and 10% of background). Corrected postions of hot spots for measured data. From sinogram fitting and timing curves the estimated amount of background is 30 % for 1.4 mm Si and 0 % for 1 mm Si. Possible that background is wrong?

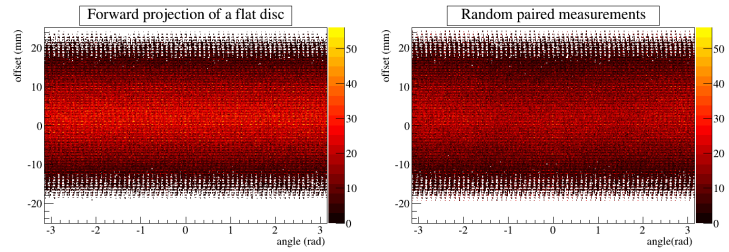

Figure 12: Two estimates of background. LEFT for forward projection of a flat disc, RIGHT for random matches from the data. A slight mismatch in the central region (independent of angles, around 0 offset) is observed. The random matches match the sensitivity, which back projects to non-uniform image.

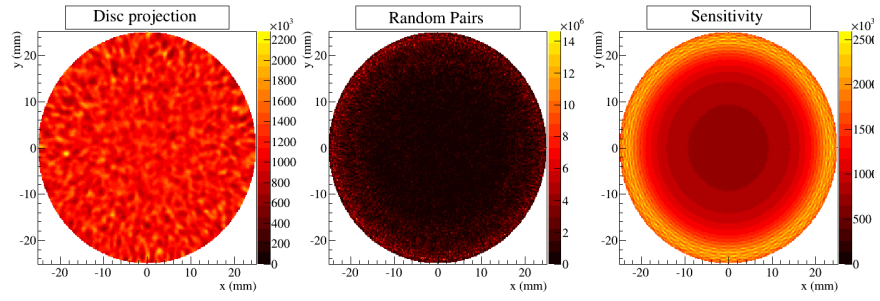

Figure 13: Comparison of images, reconstructed for different background models. Left: Reconstruction of a forward projected flat disc. Middle: Reconstruction of a sinogram from mis-matched events. Right: Reconstruction of pure sensitivity.

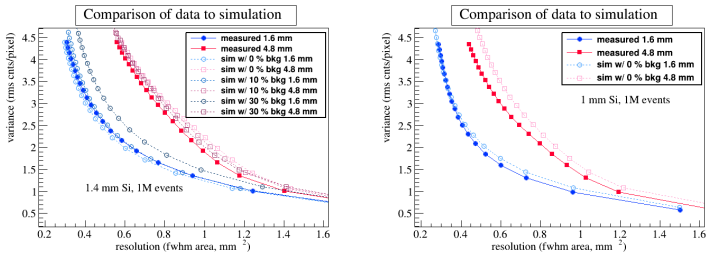

Figure 14: Comparison of simulation and real data. For 1.4 mm (LEFT) and 1 mm Si(RIGHT), 10 samples of 1M events, two rod diameters and different amount of added background (no background and up to 30% for Si-BGO data; total number of counts was kept constant). Corrected postions of hot spots for measured data. Using sensitivity as background estimate. Also, as a measure of variance the total variance of the image is used therefore equal for both rod diameters.